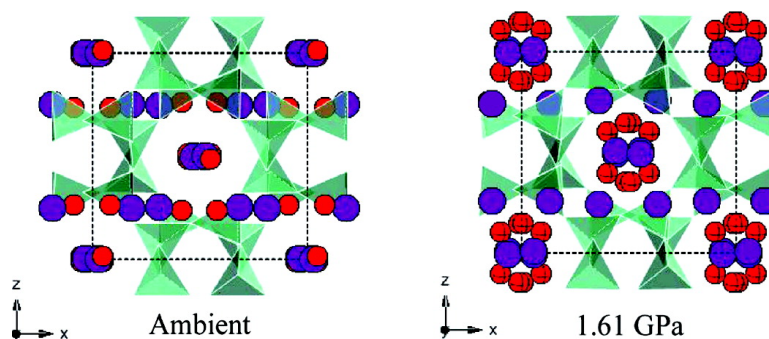## Article

Pressure-Induced Hydration and Order−Disorder Transition in a Synthetic Potassium Gallosilicate Zeolite with Gismondine Topology

Yongjae Lee, Sun Jin Kim, Chi-Chang Kao, and Thomas Vogt

Ambient   1.61 GPa

More About This Article

Additional resources and features associated with this article are available within the HTML version:

- Supporting Information
- Access to high resolution figures
- Links to articles and content related to this article
- Copyright permission to reproduce figures and/or text from this article

View the Full Text HTML

Pressure-Induced Hydration and Order−Disorder Transition in a Synthetic Potassium Gallosilicate Zeolite with Gismondine Topology

Yongjae Lee,*,† Sun Jin Kim,‡ Chi-Chang Kao,§ and Thomas Vogt‖

Department of Earth System Sciences, Yonsei University, Seoul 120-749, Korea, Nano-Materials Research Center, Korea Institute of Science and Technology, Seoul, 136-791, Korea, National Synchrotron Light Source, Brookhaven National Laboratory, Upton, New York 11973, and NanoCenter and Department of Chemistry and Biochemistry, University of South Carolina, Columbia, South Carolina 29208

Received September 28, 2007; E-mail: yongjaelee@yonsei.ac.kr

Abstract: Two high-pressure phases of a potassium gallosilicate with a gismondine framework (K−GaSi-GIS) were characterized using Rietveld refinements of in-situ high-pressure, high-resolution synchrotron X-ray powder diffraction data. The observed response of the K−GaSi-GIS framework under hydrostatic pressure is a gradual flattening of the so-called "double crankshaft" structural chain units. At pressures below 1.0(1) GPa, additional water molecules from the hydrostatic pressure-transmitting medium are inserted into the potassium-water guest network ("pressure-induced hydration") resulting in a "super-hydrated" high-pressure phase I. As the flattening of the double crankshaft structural units in the GIS framework continues above 1.6 GPa, the ellipticity of the cross-linking 8-ring windows is reduced below a certain threshold, and a disordering of the potassium-water guest structure along the 8-ring channel, characteristic of a disordered high-pressure phase II, is observed. The concerted framework distortion and guest network disordering accommodates the increased hydration level while maintaining the seven-fold coordination environment of the potassium cations to framework oxygen atoms and water molecules. We have thus established the atomistic details of a guest−host order−disorder transition under pressure-induced hydration conditions in a zeolite with GIS framework and compared it to other zeolites during pressure-induced hydration. We find that the structural changes mediated by the extra-framework cations and their coordination environment under PIH conditions are at the core of these different mechanisms and are driving the changes in the ellipticity of pore openings, order−disorder and disorder−order transitions, and framework distortions.

Introduction

The effect of hydrostatic pressure on zeolites was initially explored by Hazen.[1,2] Pressure-induced hydration in natrolite was initially proposed by Belitsky et al.[3] However, reliable structural models of zeolites under pressure were only recently determined using high-pressure, high-resolution synchrotron X-ray and neutron powder diffraction and allowed the experimental confirmation of pressure-induced hydration, where small molecules such as water and alcohols used as the pressure-transmitting medium are inserted into the pores of zeolites under pressure resulting in "super-hydrated" zeolites.[4−13] The pressure-induced hydration observed in the fibrous zeolites with a natrolite framework (NAT-type)[8,10,11,14] and other framework structures such as defect pyrochlores[15,16] demonstrates that the distribution and coordination of nonframework species can be noticeably altered when applying hydrostatic pressures. This is not surprising since it is well-established that ion exchange and hydration/dehydration are coupled reactions in zeolites.[17] In the mineral natrolite itself ($Na_{16}Al_{16}Si_{24}O_{80}$ $16H_2O$), the structural models based on refinements of synchrotron X-ray and neutron powder diffraction data obtained under pressure[5,8,10] indicates

† Yonsei University.
‡ Korea Institute of Science and Technology.
§ Brookhaven National Laboratory.
‖ University of South Carolina.
(1) Hazen, R. M. *Science* **1983**, *219*, 1065.
(2) Hazen, R. M.; Finger, L. W. *J. Appl. Phys.* **1984**, *56*, 1838.
(3) Belitsky, I. A.; Fursenko, B. A.; Gubada, S. P.; Kholdeev, O. V.; Seryotkin, Y. V. *Phys. Chem. Miner.* **1992**, *18*, 497.
(4) Colligan, M.; Forster, P. M.; Cheetham, A. K.; Lee, Y.; Vogt, T.; Hriljac, J. A. *J. Am. Chem. Soc.* **2004**, *126*, 12015.
(5) Colligan, M.; Lee, Y.; Vogt, T.; Celestian, A. J.; Parise, J. B.; Marshall, W. G.; Hriljac, J. A. *J. Phys. Chem. B* **2005**, *109*, 18223.
(6) Gatta, G. D.; Wells, S. A. *Phys. Chem. Miner.* **2006**, *33*, 243.
(7) Greaves, G. N.; Meneau, F.; Sapelkin, A.; Colyer, L. M.; Gwynn, I. A.; Wade, S.; Sankar, G. *Nat. Mater.* **2003**, *2*, 622.

(8) Lee, Y.; Hriljac, J. A.; Vogt, T.; Parise, J. B.; Artioli, G. *J. Am. Chem. Soc.* **2001**, *123*, 12732.
(9) Lee, Y.; Lee, H. H.; Lee, D. R.; Shin, T. J.; Choi, J. Y.; Kao, C. C. *J. Am. Chem. Soc.* **2007**, *129*, 4888.
(10) Lee, Y.; Vogt, T.; Hriljac, J. A.; Parise, J. B.; Artioli, G. *J. Am. Chem. Soc.* **2002**, *124*, 5466.
(11) Lee, Y.; Vogt, T.; Hriljac, J. A.; Parise, J. B.; Hanson, J. C.; Kim, S. J. *Nature* **2002**, *420* (6915), 485.
(12) McMillan, P. F. *Nat. Mater.* **2002**, *1*, 19.
(13) Seryotkin, Y. V.; Bakakin, V. V.; Fursenko, B. A.; Belitsky, I. A.; Joswig, W.; Radaelli, P. G. *Eur. J. Mineral.* **2005**, *17*, 305.
(14) Lee, Y.; Hriljac, J. A.; Parise, J. B.; Vogt, T. *Am. Mineral.* **2005**, *90*, 252.
(15) Perottoni, C. A.; Jornada, J. A. H. d. *Phys. Rev. Lett.* **1996**, *78*, 2991.
(16) Barnes, P. W.; Woodward, P. M.; Lee, Y.; Vogt, T.; Hriljac, J. A. *J. Am. Chem. Soc.* **2003**, *125*, 4572.
(17) Breck, D. W. *Zeolite Molecular Sieves: Structure, Chemistry and Use*; Krieger: Malabar FL, 1984.
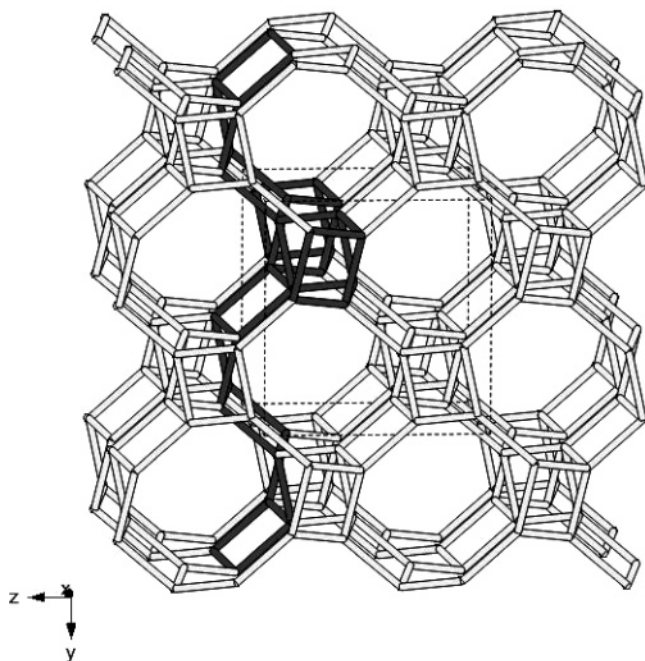
Figure 1. Stick representation of the gismondine-type gallosilicate framework structure viewed along [100]. The cross-linking of the two double crankshaft chain units is emphasized with dark gray. Vertices correspond to T (Ga or Si) atoms. Framework oxygen atoms and extra-framework species are omitted for clarity. Dotted lines outline a unit cell.

that under pressure in the presence of water which can penetrate the pores an auxetic framework distortion based on a "rotating squares"-mechanism[18,19] leads to a volume expansion and hydration under pressure ("superhydration").[10,11,14] It has recently been shown that natrolite is indeed such an "auxetic" material.[20] Auxetic materials have negative Poisson's ratios leading to a thinning when compressed and a fattening when stretched. In natrolite this behavior is achieved by the concerted rotation of the semirigid structural subunits which increase the pore size as shown in our structural work.[8,10] In other large-pore zeolites such as faujasite and zeolite A, pressure-induced hydration is a more continuous process which alters the framework's compressibility and results in essentially disordered water networks within the nanometer-size pores.[4,9,21] In order to understand the effects of pressure-induced hydration in different framework types, we have investigated a gismondine (GIS) type Ga−Si zeolite ($K_{5.76}Ga_{5.76}Si_{10.24}O_{32} \cdot 9.9H_2O$) using a diamond-anvil cell to create hydrostatic pressures and high-resolution synchrotron X-ray powder diffraction data to examine the structural changes.

The framework of a GIS-type zeolite is composed of two "double crankshaft" chains of tetrahedrons that are connected perpendicular to each other (Figure 1).[22−24] The resulting three-dimensional framework possesses interconnected pores and channels that are accessed through 8-ring openings. In the mineral gismondine (ideally, $Ca_4Al_8Si_8O_{32} \cdot 16H_2O$), the silicon

and aluminum cations are in the center of oxygen tetrahedrons which are either ordered or disordered depending on the Si/Al ratio: they are ordered when the ratio is close to unity[22,25] and disordered when Si-rich.[26,27] Members of this structural family with GIS-type frameworks containing Be-, P-, Ga-, and GeO_4 tetrahedra have also been reported.[28−30] There are many different exchangeable nonframework cations which control the zeolitic water content and other physical properties.[31,32] The varied framework chemistry, coupled with the easy ion-exchange properties, are a sign that the GIS-type framework is quite adaptable. In fact, numerous structural studies on GIS-type zeolites have been reported as a function of cation substitution and dehydration. These studies reveal the largest range of unit cell variations and symmetries thus far encountered in a single-framework-type zeolite.[31,33,34] However, the structural effect of hydrostatic pressure on the gismondine-type framework and its cation-water sub lattice remains unknown. Hydration will strengthen the effective dielectric medium and reduce the electrostatic repulsion between cations thereby increasing their mobility. A recent computational study suggests that an order−disorder reorganization of the $Ca−H_2O$ guest network could occur in the mineral gismondine under pressure.[35] We report here on the pressure-induced structural changes of a synthetic potassium gallosilicate with such a gismondine framework using detailed Rietveld analysis based on in-situ high-pressure synchrotron X-ray powder diffraction data and establish a mechanism of pressure-induced hydration and the concomitant order−disorder transition and framework distortion.

Experimental Methods

High-Pressure Synchrotron X-ray Powder Diffraction. The synthesis of K−GaSi-GIS was described in detail by Tripathi et al.[30] Initial characterization and screening to find suitable experimental conditions were performed using a symmetric diamond-anvil cell and an imaging plate detector at 5A-HFMS beamline at Pohang Accelerator Laboratory (PAL). In situ high-pressure high-resolution synchrotron X-ray powder diffraction experiments were performed at the X7A beamline at the National Synchrotron Light Source (NSLS) at Brookhaven National Laboratory (BNL). The primary white beam from the bending magnet was focused in the horizontal plane by a triangular Si (111) monochromator bent to a cylindrical curvature by applying a load to the crystal tip, creating a ∼200 μm focal spot of monochromatic X-rays with a wavelength of 0.6474 Å. A gas-proportional position-sensitive detector (PSD) gated on the Kr-escape peak was used to collect high-resolution powder diffraction data ($\Delta d/d \sim 10^{-3}$).[36] The PSD covered 4° in 2θ and was stepped in 0.25° intervals over the angular range of 3.5−35.5° with counting times of 90−150 s per step. The wavelength of the incident beam was determined from a CeO_2 standard (SRM 674).

(18) Grima, J. N.; Zammit, V.; Gatt, R.; Alderson, A.; Evans, K. E. *Phys. Status Solidi B* **2007**, *244* (3), 866.
(19) Williams, J. J.; Smith, C. W.; Evans, K. E. *Chem. Mater.* **2007**, *19*, 2423.
(20) Grima, J. N.; Gatt, R.; Zammit, V.; Williams, J. J.; Evans, K. E.; Alderson, A.; Walton, R. I. *J. Appl. Phys.* **2007**, *101*, 086102.
(21) Arletti, R.; Ferro, O.; Quartieri, S.; Sani, A.; Tabacchi, G.; Vezzalini, G. *Am. Mineral.* **2003**, *88*, 1416.
(22) Fischer, K. *Am. Mineral.* **1963**, *48*, 664.
(23) Breck, D. W.; Acara, N. A. U.S. Patent *711*,565, 1968.
(24) Baerloch, C; Meier, W. M. *Z. Kristallogr.* **1972**, *135*, 339.

(25) Alberti, A.; Vezzalini, G. *Acta Crystallogr.* **1979**, *35*, 2866.
(26) McCusker, L. B.; Baerlocher, C.; Nawaz, R. *Z. Kristallogr.* **1985**, *171*, 281.
(27) Artioli, G. *Am. Mineral.* **1992**, *77*, 189.
(28) Feng, P.; Bu, X.; Stucky, G. D. *Nature* **1997**, *388*, 735.
(29) Johnson, G. M.; Tripathi, A.; Parise, J. B. *Chem. Mater.* **1999**, *11*, 10.
(30) Tripathi, A.; Parise, J. B.; Kim, S. J.; Lee, Y. J.; Uh, Y. S. *Acta Crystallogr., Sect. C* **2001**, *57*, 344.
(31) Bauer, T.; Baur, W. H. *Eur. J. Mineral.* **1998**, *10* (1), 133.
(32) Dyer, A.; Heywood, B.; Szyrokyj, N. *Microporous Mesoporous Mater.* **2006**, *92*, (1−3), 161.
(33) Celestian, A. J.; Parise, J. B.; Goodell, C.; Tripathi, A.; Hanson, J. *Chem. Mater.* **2004**, *16* (11), 2244.
(34) Vezzalini, G.; Quartieri, S.; Alberti, A. *Zeolites* **1993**, *13*, 34.
(35) Betti, C.; Fois, E.; Mazzucato, E.; Medici, C.; Quartieri, S.; Tabacchi, G.; Vezzalini, G.; Dmitriev, V. *Microporous Mesoporous Mater.* **2007**, *103*, 190.
(36) Smith, G. C. *Synchrotron Radiat. News* **1991**, *4*, 24.

Table 1. Rietveld Refined Structural Models of K−GaSi-GIS at Hydrostatic Pressures at Room Temperature[a]

		ambient	0.42 GPa	0.94 GPa	1.61 GPa	2.23 GPa	2.80 GPa
S.G.		$I4_1/a$	$I4_1/a$	$I4_1/a$	$I4_1/a$	$I4_1/a$	$I4_1/a$
a (Å)		10.0668(3)	10.0517(2)	10.0548(3)	10.0835(3)	10.0741(4)	10.0621(5)
c (Å)		9.6466(3)	9.6148(3)	9.5433(3)	9.4084(4)	9.3033(5)	9.2185(5)
V (Å³)		977.58(7)	971.44(7)	964.82(8)	956.61(9)	944.2(1)	933.3(1)
H_2O/u.c.		9.9(1)	9.7(1)	11.6(1)	11.9(2)	12.0(3)	12.4(4)
obs./refs/var.		3009/194/26	3009/192/26	3009/194/26	3009/194/25	3009/192/25	3009/188/26
R_{F2}		0.128	0.136	0.110	0.104	0.115	0.140
$_wR_p/\chi^2$		0.033/4.98	0.030/6.13	0.025/7.43	0.028/7.38	0.029/8.69	0.029/5.31
T^b	x	0.3244(1)	0.3246(1)	0.3240(1)	0.3241(1)	0.3253(1)	0.3253(2)
	y	0.6248(1)	0.6250(1)	0.6245(1)	0.6246(1)	0.6258(1)	0.6258(2)
	z	0.0899(1)	0.0901(1)	0.0896(1)	0.0897(1)	0.0909(1)	0.0909(2)
	$U_{(iso)}$	0.0287(6)	0.0181(6)	0.0170(5)	0.0161(6)	0.0202(7)	0.0130(7)
O1	x	0.3237(6)	0.3246(6)	0.3175(5)	0.3180(7)	0.3155(7)	0.314(1)
	y	0.7933(4)	0.7945(4)	0.7916(4)	0.7887(7)	0.7875(8)	0.788(1)
	z	0.0739(7)	0.0731(6)	0.0737(6)	0.0639(7)	0.0655(8)	0.067(1)
	$U_{(iso)}{}^c$	0.042(2)	0.039(2)	0.038(2)	0.053(2)	0.041(2)	0.047(3)
O2	x	0.3091(6)	0.3114(6)	0.3181(6)	0.3344(7)	0.3382(8)	0.340(1)
	y	0.5610(5)	0.5597(5)	0.5554(5)	0.5523(6)	0.5534(7)	0.554(1)
	z	0.9277(5)	0.9285(5)	0.9280(5)	0.9299(8)	0.9339(9)	0.932(1)
K[d]	x	0.186(1)	0.178(1)	0.162(1)	0.1354(4)	0.1300(4)	0.1282(4)
	y	0.721(2)	0.718(1)	0.720(1)	0.6909(4)	0.6854(4)	0.6836(4)
	z	0.752(1)	0.743(1)	0.742(1)	0.7402(4)	0.7348(4)	0.7329(4)
	occu.	0.360	0.360	0.360	0.360	0.360	0.360
	$U_{(iso)}{}^c$	0.084(4)	0.071(4)	0.049(3)	0.057(3)	0.034(3)	0.032(3)
W1	x	0.084(2)	0.082(2)	0.087(2)	0.011(5)	−0.007(3)	−0.029(5)
	y	0.700(2)	0.704(2)	0.677(2)	0.655(3)	0.644(3)	0.651(3)
	z	0.736(1)	0.734(1)	0.750(1)	0.853(5)	0.904(4)	0.895(5)
	occu.	0.621(9)	0.604(9)	0.724(9)	0.190(6)	0.265(9)	0.283(9)
	$U_{(iso)}{}^c$	0.113(9)	0.119(9)	0.133(9)	0.057(3)	0.034(3)	0.032(3)
W2[e]	x				0.1354(4)	0.1300(4)	0.1282(4)
	y				0.6909(4)	0.6854(4)	0.6836(4)
	z				0.7402(4)	0.7348(4)	0.7329(4)
	occu.				0.554(9)	0.48(1)	0.49(1)

[a] Estimated standard deviations are in parentheses. Tetrahedral T−O and O−O distances are restrained to 1.685(1) Å and 2.752(5) Å, respectively. [b] Gallium and silicon occupancies for the tetrahedral (T) site are fixed to 0.36 and 0.64, respectively. [c] Isotropic displacement factors are constrained to be equal for the framework oxygen atoms (ambient to 0.94 GPa models), or for the framework oxygen atoms and the nonframework species (1.61 to 2.80 GPa models). [d] Potassium occupancy is fixed to 0.36 [e] Mixed K−W2 site (W2 position is constrained to be same with that of K, while its occupancy is refined).

A modified Merrill−Bassett diamond anvil cell (DAC) was used for the high-pressure experiments, equipped with two type-I diamond anvils (culet diameter of 700 μm) and tungsten−carbide supports. A stainless-steel foil of 250 μm thickness was pre-indented to a thickness of about 100 μm, and a 250 μm hole was obtained by electrospark erosion. A powdered sample of K−GaSi-GIS from the batch used for the single crystal study was placed in the gasket hole together with some ruby chips for in situ pressure measurements. A methanol/ethanol/water (16:3:1 by volume) mixture was used as hydrostatic pressure-transmitting medium in the DAC. The pressure the sample was exposed to in the DAC was measured by detecting the shift in the R1 emission line of the included ruby chips (precision: ±0.05 GPa).[37] The sample was equilibrated for about 10 min in the DAC at each measured pressure. The initial sample to beam alignment was achieved by using a prefocused microscope, and then a 200 μm diameter pinhole was inserted to the center of the aligned sample to avoid any gasket contamination in the measured diffraction data. After each powder diffraction pattern was collected, the pressure was increased in increments of ∼0.5 GPa.

The structural refinements were performed using the Rietveld method and the GSAS suite of programs.[38] The starting model of the hydrated K−GaSi-GIS was taken from a previous single crystal study.[30] The background was fitted by a linear interpolation between selected positions in 2θ. The pseudo-Voigt profile function proposed by Thompson et al.[39] was used to model the observed Bragg peaks. In order to reduce the number of parameters, isotropic displacement factors were refined by grouping the framework oxygen atoms and the nonframework cations and water oxygen atoms, respectively. Geometrical soft-restraints on the T−O (T = Ga,Si) and O−O bond distances of the tetrahedra were applied: the T−O distances were restrained to a value of 1.685 ± 0.001 Å and the O−O distances to 2.752 ± 0.005 Å, assuming bond lengths for Si−O and Ga−O to be 1.61 Å and 1.82 Å, respectively. Furthermore, a random occupation of Si and Ga over the tetrahedral sites and a linear variation of the Si/Ga−O distances based on the previously established cation ratio of Si/Ga = 1.78 were introduced into the model as constraints.[30] The potassium occupancy was also fixed to 5.76 per unit cell based on the previous single crystal study. Water molecules were modeled using only the oxygen scattering factor. In the final stages of the refinements, convergence was achieved by refining simultaneously all profile parameters, scale factor, lattice constants, 2θ zero, the atomic positional and thermal displacement parameters, and occupancy factors for the water oxygen atoms. A typical Rietveld full-profile fit of K−GaSi-GIS at high pressure is shown in the figure in Supporting Information. The final refined parameters are summarized in Table 1, and selected bond distances and angles are listed in Table 2.

Results and Discussion

An anisotropic compression behavior (Figure 2) can be seen by inspecting the powder diffraction pattern which reveals that the shifts of the peaks in 2θ with increasing pressure are not

(37) Bell, P. M.; Mao, H. K. Absolute pressure measurements and their comparison with the ruby fluorescence (R1) pressure scale to 1.5 Mbar. In *Carnegie Institute Washington Year Book*; 1979; Vol. 78, pp 665.
(38) Toby, B. H. *J. Appl. Crystallogr.* **2001**, *34*, 210.
(39) Thompson, P.; Cox, D. E.; Hastings, J. B. *J. Appl. Crystallogr.* **1987**, *20*, 79.

Table 2. Selected Interatomic Distances (Å) and Angles (deg) of K−GaSi-GIS at Hydrostatic Pressures at Room Temperature[a]

	ambient	0.42 GPa	0.94 GPa	1.61 GPa	2.23 GPa	2.80 GPa
T−O1	1.703(4)	1.711(4)	1.689(4)	1.673(7)	1.649(8)	1.653(8)
T−O1	1.653(6)	1.639(6)	1.686(5)	1.750(7)	1.743(8)	1.733(9)
T−O2	1.699(5)	1.693(5)	1.692(5)	1.674(7)	1.637(8)	1.637(9)
T−O2	1.735(6)	1.718(6)	1.651(6)	1.584(7)	1.605(8)	1.592(9)
av T4−O[b]	1.698(3)	1.690(3)	1.680(3)	1.670(4)	1.659(4)	1.654(4)
T−O1−T	139.1(4)	138.7(4)	137.8(4)	134.0(4)	133.7(5)	133.9(6)
T−O2−T	135.4(3)	136.9(3)	141.0(3)	147.9(5)	149.3(5)	148.6(6)
K−O1	3.15(1)	3.04(1)	3.022(9)	2.83(1)	2.73(1)	2.69(1)
			3.20(1)	2.91(1)	2.86(1)	2.84(1)
K−O2	2.65(2)	2.74(1)	2.89(1)	3.03(1)	3.10(1)	3.10(1)
	3.17(2)	3.17(1)	2.79(1)	3.06(1)	3.08(1)	3.06(1)
	2.80(2)	2.78(1)				
K−K[e]	1.43(2)	1.59(2)	1.88(2)			
K−W2 (W2−W2)[c]				2.98(1)	2.925(3)	2.905(4)
				2.61(1)	2.76(1)	2.81(1)
K−W1(W2−W1)[d]	2.83(2)	2.73(2)	2.71(1)	3.05(4)	2.86(3)	3.02(4)
	2.46(3)	2.55(3)	2.73(2)	2.80(3)	2.69(3)	2.72(3)
	3.09(2)	3.15(2)	2.87(1)	2.39(4)	2.64(3)	2.45(4)
K−W1[e]	1.06(2)	0.98(2)	0.87(2)	1.69(5)	1.21(4)	1.22(4)
W1−O1	2.85(2)	2.87(2)	2.59(2)	2.76(3)	2.97(3)	2.99(4)
W1−W1	1.96(3)[e]	1.90(3)[e]	2.30(2)[e]	1.43(4)[e]	1.60(5)[e]	1.51(4)[e]
	3.02(2)	3.03(2)	2.88(2)			

[a] Estimated standard deviations are in parentheses. Tetrahedral T−O and O−O distances are restrained to 1.685(1) Å and 2.752(5) Å, respectively. [b] Standard deviations computed using $\sigma = 1/n[\sum_{i=1}^{n} \sigma i^2]^{1/2}$. [c] Possible H_2O-H_2O distances from the mixed K−W2 site in the models above 1.61 GPa. [d] Possible H_2O-H_2O distances between the mixed K−W2 site and the W1 site in the models above 1.61 GPa. [e] Simultaneous occupancy is excluded or indicates partial (or disordered) hydrogen bonding.
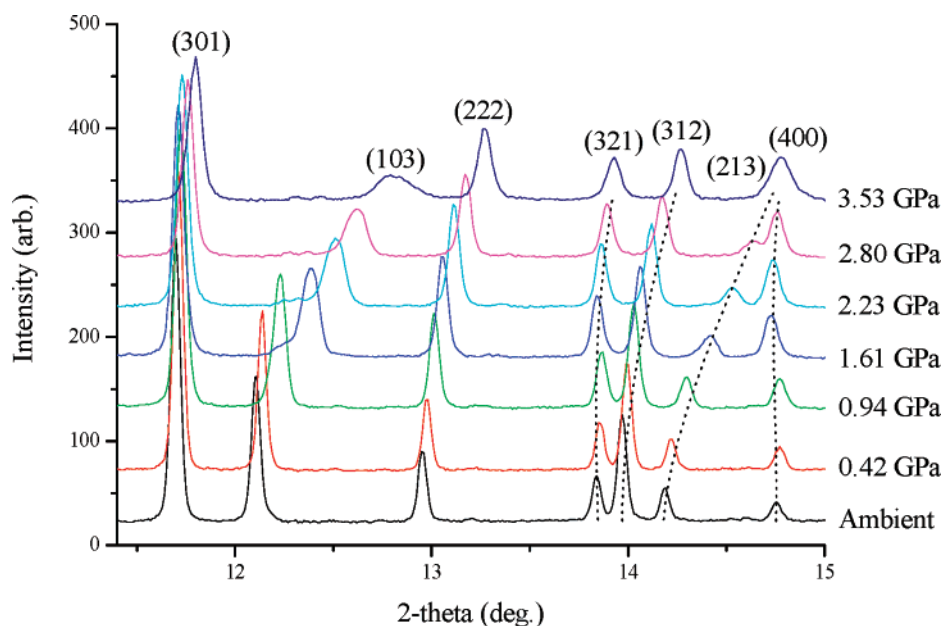

Figure 2. Details of the changes in the synchrotron X-ray powder diffraction patterns observed for K−GaSi-GIS as a function of hydrostatic pressure mediated by alcohol and water mixture. Dotted lines are guides to the eyes to show progressive shifts in Bragg peak positions.

monotonic and not independent of the Miller indices (*hkl*). In fact, the peaks with lower *l*'s (i.e. 301, 321) shift to lower 2θ in the early stages of the compression of the structure below pressures of 1.6 GPa (Figure 2). The evolution of the tetragonal *a*- and *c*-unit cell lengths of the K−GaSi-GIS, derived from a full profile fitting procedure as described in the Experimental Methods, clearly indicates a change in the evolution of the *a*-unit cell parameter at pressure near 1 GPa, where an increase in the axis length by ca. 0.3% is observed (Figure 3a). This, coupled with the gradual decrease of the *c*-axis length, leads to a change in the slope of the overall volume compression (Figure 3b). The volume compressibility was determined using the Birch−

Murnaghan equation of state (BM-EoS), which is based upon the assumption that the high-pressure strain of a solid can be expressed as a Taylor series of the Eulerian strain,

$$f = [(V_0/V)^{2/3} - 1]/2$$

(V_0 and V represent the unit-cell volume, under ambient and high-pressure conditions, respectively). Expansion in the Eulerian strain yields the following isothermal equation-of-state:

$$P(f) = 3K_0 f(1 + 2f)^{5/2} \{1 + 3/2(K' - 4)f +$$
$$3/2[K_0 K'' + (K' - 4)(K' - 3) + 35/9]f^2 + ...\}$$
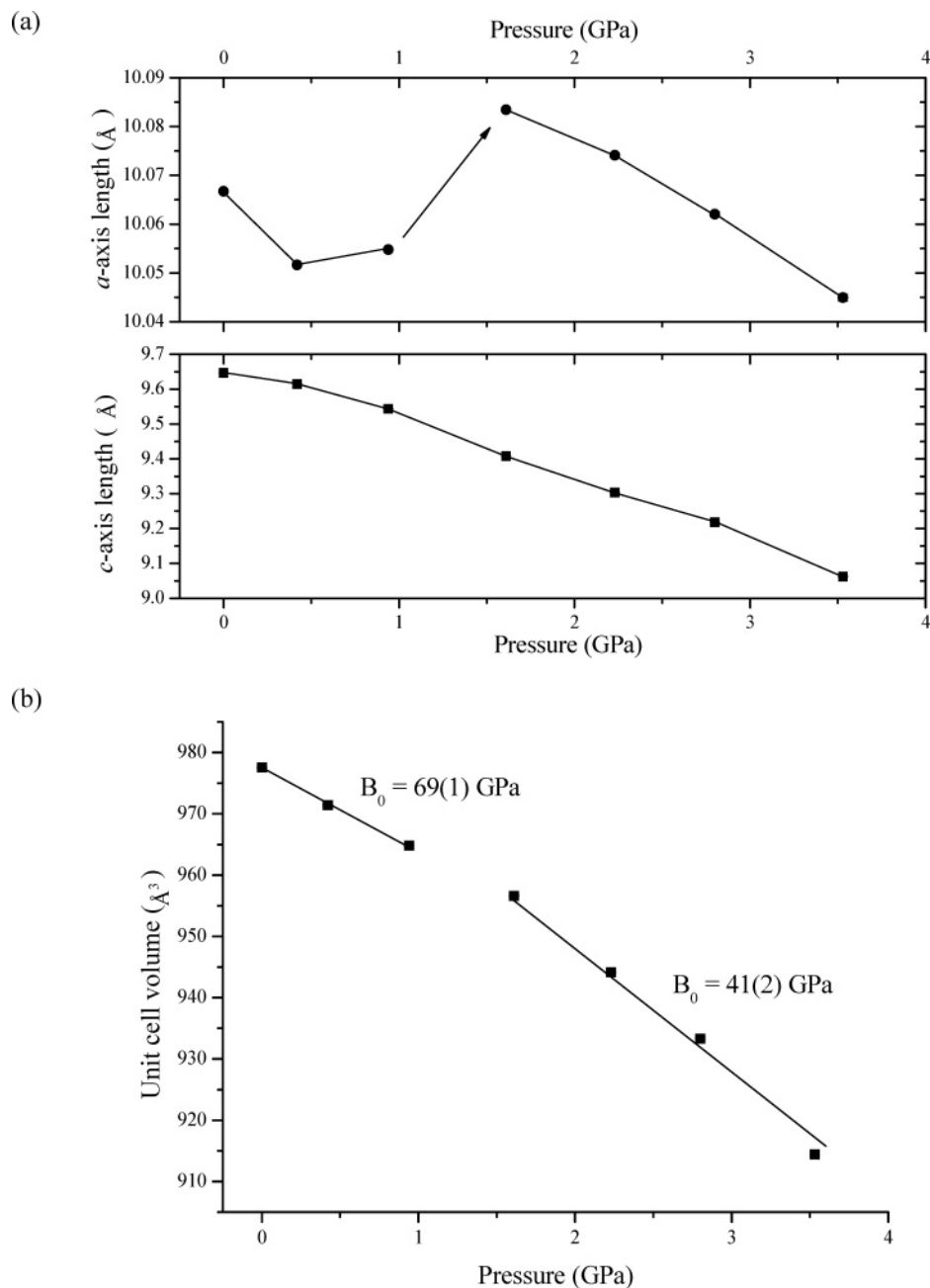
(a)

(b)

Figure 3. Changes in (a) the unit cell edge lengths and (b) volume of K−GaSi-GIS as a function of the applied hydrostatic pressures.

where K_0 represents the bulk modulus, defined as $K_0 = -V_0(\partial P/\partial V)_{P=0} = 1/\beta$, where β is the volume compressibility coefficient and K' and K'' represent the first and second derivatives of the bulk modulus with respect to pressure

$$K' = \partial K_0/\partial P; \quad K'' = \partial^2 K_0/\partial P^2$$

Due to the limited pressure range investigated and the small volume reduction at the maximum pressure (less than 7%), the $P-V$ data of K−GaSi-GIS were fitted using a truncated second-order BM-EoS with K' fixed at 4.[40] In addition, to account for the increased compressibility above 1.6 GPa, the $P-V$ data were divided into two data sets above and below 1.6 GPa, hereafter referred to as phase I and phase II. The volume at 1.6 GPa was

(40) Hazen, R. M.; Finger, L. W. *Comparative Crystal Chemistry*; John Wiley & Sons: New York, 1982.

used as V_0 to determine the bulk modulus of phase II. The derived bulk moduli are 69(1) GPa and 41(2) GPa for phases I and II, respectively. The unusual increase of the compressibility at pressures above 1.6 GPa indicates that the structure of the high-pressure phase II of K−GaSi-GIS undergoes changes in the water content and/or a rearrangement of the cation−water network, facilitating a framework distortion.

The crystal chemical evolution of the K−GaSi-GIS under hydrostatic pressure conditions with pore-penetrating molecules such as water and alcohols present was determined using Rietveld analyses (Tables 1−2). Close to the pressure where a significant change is observed in the *a*-unit cell length, a concomitant increase of the water content is also observed (Figure 4). From ambient conditions up to 1 GPa, the water content increases from 9.9(1) to 11.6(1) water molecules per unit cell. The distribution of the nonframework species, however,
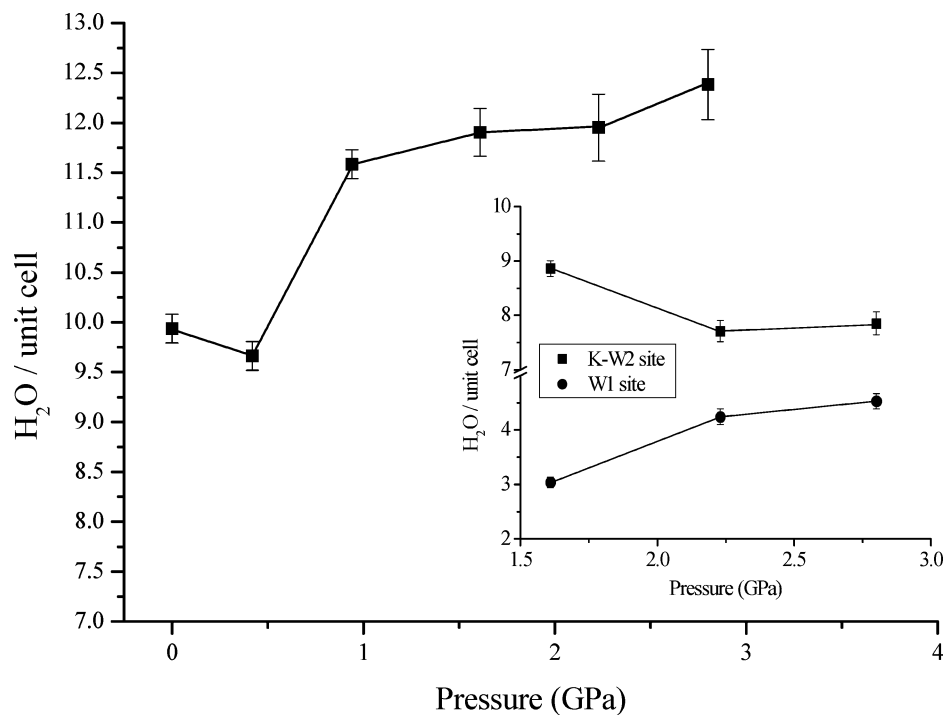
Figure 4. Pressure-induced hydration of K−GaSi-GIS. Migration of the water molecules from the mixed K−W2 site to the W1 site is shown as an inset. Lines are guides to the eyes.
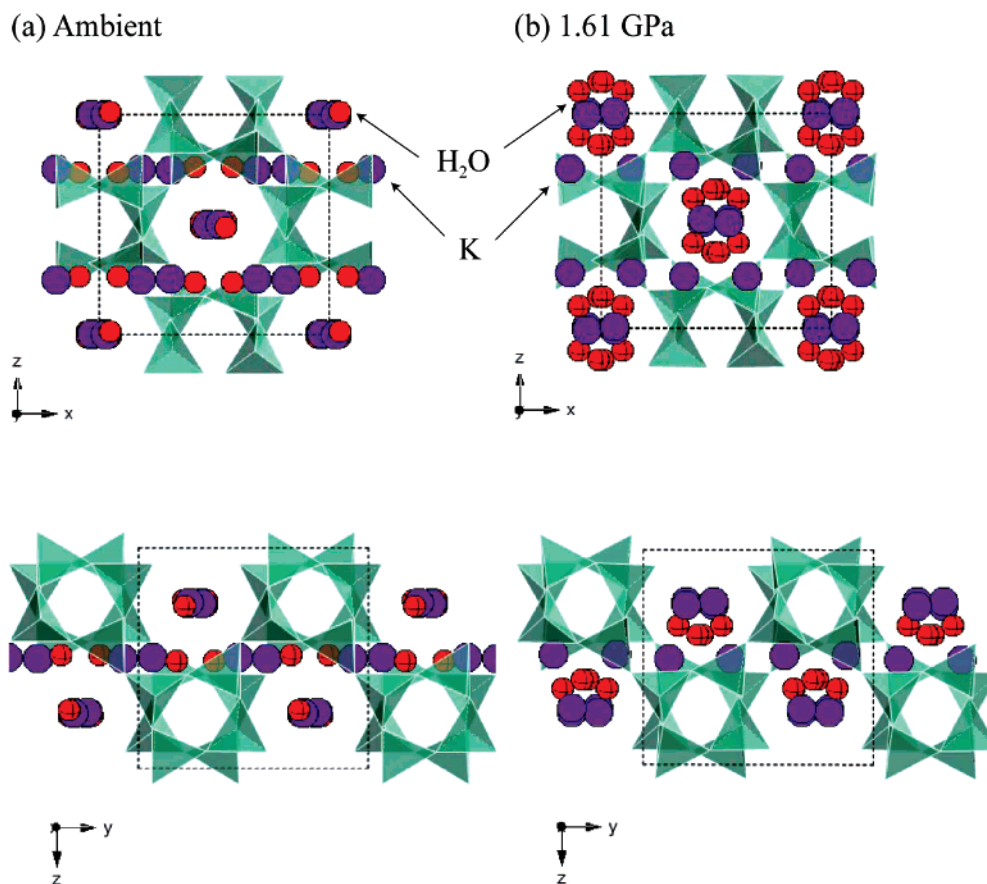

Figure 5. Refined structural models of K−GaSi-GIS (a) at ambient condition and (b) at 1.6 GPa, viewed along the *b*-axis (upper) and along the *a*-axis (lower). TO$_4$ (T = Ga/Si) tetrahedra are shown as translucent polyhedra, and red and purple circles represent oxygen atoms of water molecules and potassium cations, respectively. In the model at 1.6 GPa, the purple circles represent the mixed K−W2 site. Dotted lines outline a unit cell.

is practically not altered (Figure 5) up to pressures of 1 GPa; the potassium cations continue to occupy a separate site distinct from the W1 site that the water molecules occupy and are seven-

coordinated to four framework oxygen atoms and three water molecules with interatomic distances in the range of 2.65(2)− 3.20(1) Å and 2.46(3)−3.15(2) Å, respectively (Table 2). This
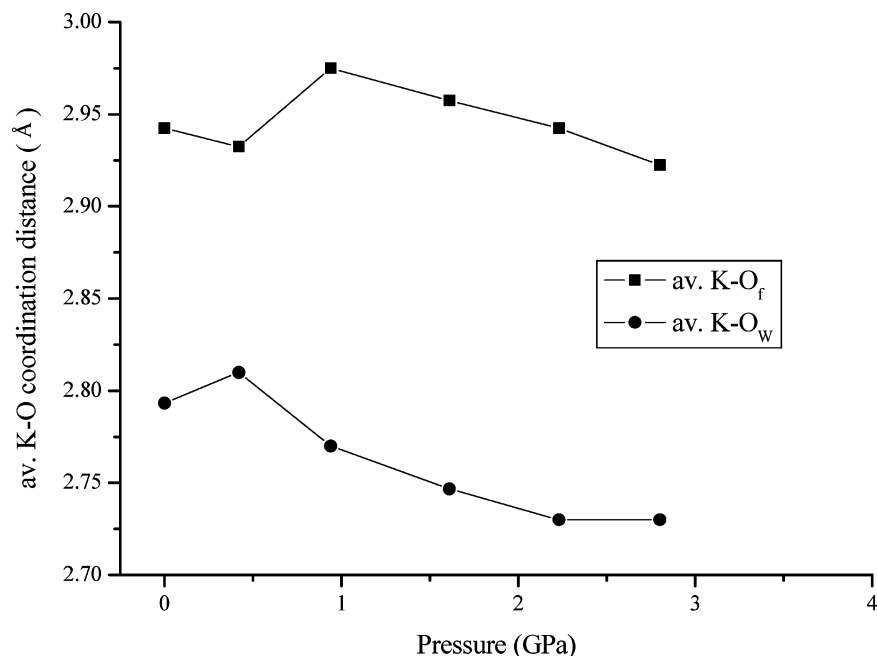
Figure 6. Pressure-induced changes in the average bond lengths of the potassium coordination polyhedra composed of four framework oxygen atoms (O_f) and three water molecules (O_W) (see Table 2).

arrangement of the potassium cations and water molecules is best described as a zigzag chain of $K-H_2O$, confined to the *ab*-plane and aligned along the direction of each 8-ring channel. Due to the topology of the gismondine framework, the potassium−water chains run parallel to each other in the *ab*-plane and are stacked at a right angle with respect to the neighboring ones along the *c*-axis (Figure 5). This type of stacking is facilitated by hydrogen bonding between water molecules in the range of 2.88(2)−3.03(2) Å, and subsequently leads to the interconnection of these individual chains to form a three-dimensional guest network (Table 2).
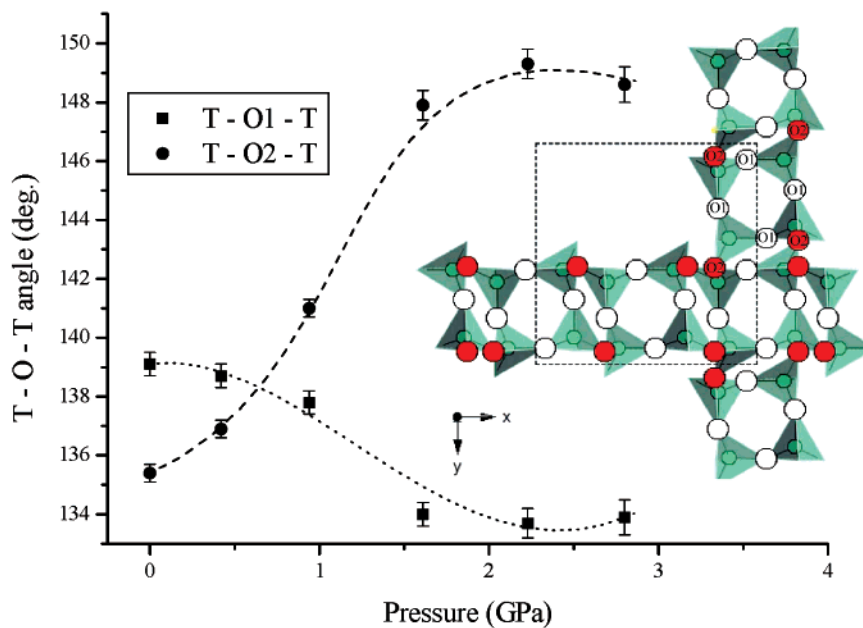
The refined structural models of phase II above 1.6 GPa differ significantly from those of phase I below 1 GPa (Figure 5). During the compression at higher pressures, the total water content remains constant as indicated by 11.9(2) H_2O per unit cell at 1.6 GPa and 12.4(4) H_2O per unit cell at 2.8 GPa; pressure-induced hydration no longer occurs. However, at pressures above 1.6 GPa, the potassium cations are now disordered with water molecules and found on a new crystallographic site (K−W2) (Table 1). The water molecules at the former W1 site are now displaced out of the *ab*-plane and located near the center of the interconnected 8-ring channels along the *a*- and *b*-axis (Figure 5). The refinement of the water occupancies at both sites was performed with the potassium occupancy at the mixed K−W2 site fixed to the experimentally established one.[30] The water molecules gradually migrate from the K−W2 site to the W1 site as the pressure increases (Figure 4). The coordination environment of the potassium cation is still composed of four framework oxygen atoms and three W1 water molecules as observed in phase I (Table 2). The arrangement of the $K-H_2O$ chain is, however, now altered due to the displacement of the W1 water molecules and develops an undulation along the *c*-axis (Figure 5). This new three-dimensional guest network is very likely the result of hydrogen bonding both within the individual $K-H_2O$ chains and in between the neighboring ones stacked at a right angle along

the *c*-axis. Under pressure the dimensionality of the water network has thus been increased. In a single chain, the water oxygen atoms of the mixed K−W2 sites are spaced within a range of 2.61(1) Å and 2.98(1) Å and hence are most likely hydrogen-bonded chain (Table 2). Interchain interactions are probably also facilitated by hydrogen bonding between the water molecules from the W1 site and the mixed K−W2 site over distances of 2.39(4)−3.05(4) Å (Table 2). A final confirmation of this hydrogen-bonded network will need to wait until high-quality neutron powder diffraction data under hydrostatic pressure will allow the location of the hydrogen atoms in this structure. We propose that the disordering of the guest network is responsible for the increased compressibility of the host lattice in the phase II at pressures above 1.6 GPa. The changes in the bond strength of the potassium coordination polyhedra also reveal an important correlation with changes in the guest chemistry and the host framework distortion (Figure 6). In phase I, pressure-induced hydration near 1 GPa, weakens the average potassium to framework oxygen (O_f) bonding, while strengthening the average potassium to water oxygen (O_W) interaction. This is similar as observed in many ambient hydration processes where nonframework cations are progressively moved toward the center of pores and away from the framework oxygen.[41] Subsequently in phase II, under increasing pressure the disordered $K-H_2O$ network increases its coupling both with the host lattice and in-between the individual chains, and a gradual shortening of the potassium−oxygen interactions with increasing framework distortion is observed under pressure (Figure 6). Overall, the potassium to water interaction is found to be stronger than the potassium to framework oxygen interaction, and this might explain the fact that the observed framework flexibility is dependent on the water content.

As expected, the framework of gismondine undergoes significant changes during the pressure-induced hydration and

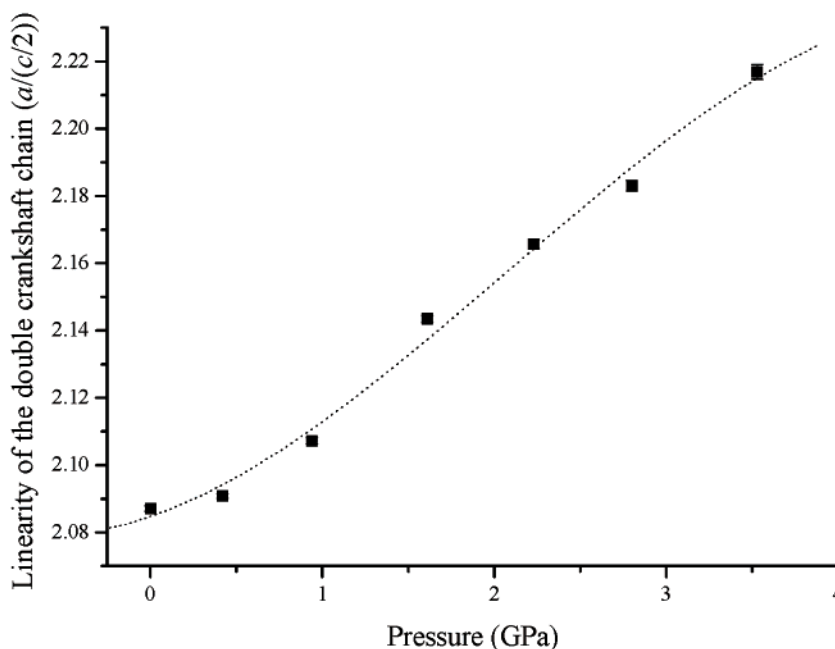(41) O'Connor, D.; Barnes, P.; Bates, D. R.; Lander, D. F. *Chem. Commun.* **1998**, 2527.

(a)

(b)

Figure 7. (a) Pressure-induced evolution of the T−O−T bridging angles and (b) concomitant changes in the linearity of the double crankshaft chain (defined by $a/(c/2)$). (Inset) Two interconnecting double crankshaft chains viewed in the *ab*-plane to illustrate the location of the bridging oxygen atoms (open circles for the O1 oxygen atoms and red circles for the O2 oxygen atoms).

the associated rearrangement of its guest network. The tetrahedral bridging angles, T−O1−T and T−O2−T, respond to pressure in an opposite manner (Figure 7a). Since the T−O1−T angle defines the opening of the parallel 4-rings while the T−O2−T angle acts as a linkage between them, the cooperative change results in a continuous increase of $a/(c/2)$ ratio, which is a measure of the "flattening" of the double crankshaft chain (Figure 7b). The gismondine framework is composed of cross-linked double crankshaft chains (Figure 1) and their "flattening" due to the continuous decrease of the *c*-unit cell length is the

major response of this framework to hydrostatic pressure. Furthermore, this gradual "flattening" of the double crankshaft chains leads to a concurrent decrease of the ellipticity of the 8-ring opening which is defined in Figure 8 as the ratio between the longest and shortest oxygen−oxygen distances within the 8-ring window. As this ratio falls below a value of 1.60 near 1.6 GPa, the zigzag chain of the K−H$_2$O confined to the *ab*-plane along the 8-ring channel transforms to a disordered K−H$_2$O chain, resulting in a novel guest network in the high-pressure phase II of the K−GaSi-GIS as described above.
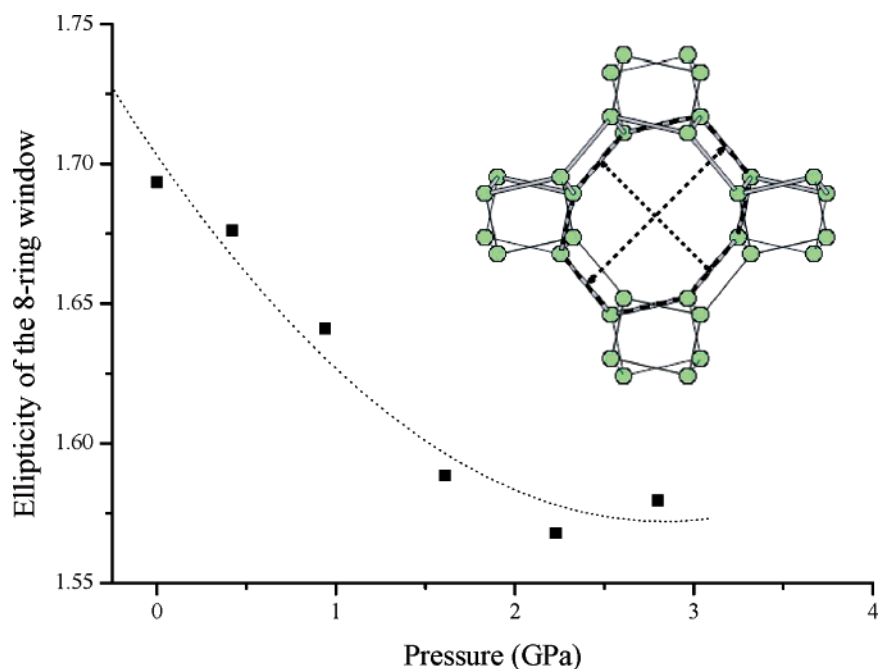
Figure 8. Changes of the ellipticity of the 8-ring window under hydrostatic pressure conditions. The ellipticity is defined by the ratio between the longest to the shortest diagonal oxygen distances of the 8-ring window (a ball and stick framework model is shown as an inset for illustration).

We have previously observed an order−disorder transition in the zeolite mesolite ($Ca_{5.33}Na_{5.33}Al_{16}Si_{24}O_{80}$ 21.3H_2O) during pressure-induced hydration.[10] At ambient conditions, a $1 \times 3 \times 1$ superstructure exists due to an ordered arrangement of the Na and Ca cations along the *b*-axis. After pressure-induced hydration near 1.5 GPa, the superlattice reflections along *b* disappear indicating that the Na and Ca sites are now disordered, and a 'natrolite' basis structure exists. Remarkably this process is reversible, and the mesolite unit cell with a $1 \times 3 \times 1$ natrolite superstructure is recovered after pressure release. The PIH phase is more compressible than the one stable at ambient conditions (80(10) GPa vs 104(1) GPa). In the mineral laumontite (Ca_4-$Al_8Si_{16}O_{48} \cdot 12\ H_2O$), on the other hand, we observe a disorder−order transition during PIH near 3 GPa.[42] Intriguingly, in this case, again a $1 \times 3 \times 1$ superstructure is implicated. The appearance of this superstructure requires an ordering of the Ca cations and/or water molecules. Again the process is reversible, and the material transforms back into its original disordered unit cell upon pressure release below 3 GPa. In the case of laumontite, we also observed a correlated distortion of the ellipticity of the channel opening within the PIH state. However, in this case, the ellipticity increases as the disorder−order transition is approached near 3 GPa.

Conclusion

We have investigated the high-pressure chemistry of a zeolite with a gismondine framework structure and established another example of the interplay between pressure-induced hydration and order−disorder transformation within a porous framework. Compared to the previously investigated pressure-induced hydration observed in mineral and synthetic natrolites, the pressure-induced hydration in the potassium gallosilicate gismondine does not involve an auxetic expansion of the pores based the "rotating squares" mechanism but rather triggers an

order−disorder transition in the K−H_2O guest sublattice. This is similar to what has been observed in mesolite upon PIH and opposite to what happens in the mineral laumontite in its PIH state. In natrolite no order−disorder transformation within the cation-water sublattice occurs during PIH.

It appears thus that the ellipticity of pore openings, order−disorder and disorder−order transitions in the guest sublattice, and framework distortions are engaged in a quite complex interplay under pressure-induced hydration conditions. These structural changes mediated by the nonframework cations and their changing coordination environment under PIH conditions are at the core of the different mechanisms observed in different classes of zeolites and establish, as in the case of dehydration and hydration under ambient conditions, their importance in exchange reactions and engineering functionalities and catalytic reactions. Tailoring microporous framework structures using PIH might lead to intriguing new opportunities and provide an exquisitely controlled size and shape selectivity which is the foundation of many industrial processes.

Supporting Information Available: Supplementary figure. This material is available free of charge via the Internet at http://pubs.acs.org.

(42) Lee, Y.; Hriljac, J. A.; Vogt, T. *Phys. Chem. Miner.* **2004**, *31*, 421.

JA077443O